Technology in Cancer Research and Treatment
ISSN 1533-0346
Volume 13, Number 5, October 2014

Standardization of Radiological Evaluation of Dynamic Contrast Enhanced MRI: Application in Breast Cancer Diagnosis

E. Furman-Haran, Ph.D.[1]
M. Shapiro Feinberg, M.D.[2]
D. Badikhi, M.Sc.[1]
E. Eyal, Ph.D.[1]
T. Zehavi, M.D.[2]
H. Degani, Ph.D.[1]*

[1]Weizmann Institute of Science, Rehovot, Israel
[2]Meir Medical Center, Kfar-Saba, Israel

www.tcrt.org
DOI: 10.7785/tcrt.2013.600263

Dynamic contrast enhanced MRI is applied as an adjuvant tool for breast cancer detection, diagnosis, and follow-up of therapy. Despite improvements through the years in achieving higher spatial and temporal resolution, it still suffers from lack of scanning and processing standardization, and consequently, high variability in the radiological evaluation, particularly differentiating malignant from benign lesions. We describe here a hybrid method for achieving standardization of the radiological evaluation of breast dynamic contrast enhanced (DCE)-magnetic resonance imaging (MRI) protocols, based on integrating the model based three time point (3TP) method with principal component analysis (PCA). The scanning and image processing procedures consisted of three main steps: 1. 3TP standardization of the MRI acquisition parameters according to a kinetic model, 2. Applying PCA to test cases and constructing an eigenvectors' base related to the contrast-enhancement kinetics and 3. Projecting all new cases on the eigenvectors' base and evaluating the clinical outcome. Datasets of overall 96 malignant and 26 benign breast lesions were recorded on 1.5T and 3T scanners, using three different MRI acquisition parameters optimized by the 3TP method. The final radiological evaluation showed similar detection and diagnostic ability for the three different MRI acquisition parameters. The area under the curve of receiver operating characteristic analysis yielded a value of 0.88 ± 0.034 for differentiating malignant from benign lesions. This 3TP+PCA hybrid method is fast and can be readily applied as a computer aided diagnostic tool of breast cancer. The underlying principles of this method can be extended to standardize the evaluation of malignancies in other organs.

Key words: Breast cancer diagnosis; Breast MRI; Dynamic contrast enhanced MRI; Three time point; Principal component analysis.

Introduction

Early detection and diagnosis of malignancy has been one of the major approaches to improve treatment and survival of cancer patients. Magnetic resonance imaging (MRI) was rapidly developed in the last three decades into a highly accurate tool for cancer detection, revealing detailed structural/anatomical information, as well as characterizing functional/physiological phenomena. One of the most widespread MRI methodologies uses Gadolinium based paramagnetic contrast agents,

Abbreviations: MRI: Magnetic Resonance Imaging; DCE: Dynamic Contrast Enhanced; PCA: Principal Component Analysis; IDC: Invasive Ductal Carcinoma; ILC: Invasive Lobular Carcinoma; DCIS: Ductal Carcinoma In Situ; TE: Echo Time; TR: Repetition Time; ROI: Region of Interest; ROC: Receiver Operating Characteristic; AUC: Area Under Curve; 3TP: Three Time Point; EV: Eigenvector; REV: Rotated Eigenvector.

*Corresponding author:
Hadassa Degani, Ph.D.
Phone: 972-8-9342017
Fax: 972-8-9346154
E-mail: Hadassa.degani@weizmann.ac.il

injected externally and followed with time by dynamic contrast enhanced (DCE)-MRI. This enables characterization of the distribution and function of the micro-vascular network in tissues (1). Specifically, DCE-MRI has become a highly effective tool for detecting and diagnosing various cancers in most parts of the body (2), including the breast and prostate (3-5). The biological/physiological basis for the distinct ability of DCE-MRI to diagnose cancer stems from the induction of pathological angiogenesis early in the course of malignant transformation. Consequently, blood vessels in cancers are highly disorganized, tortuous, dilated and leaky due to discontinuous walls and fenestrated endothelial lining (6). These changes affect blood flow and micro-vascular permeability leading to impaired delivery of nutrients and oxygen, as well as impaired fluid drainage and increased interstitial fluid pressure (7). Currently, DCE-MRI monitors the time course of the distribution of the contrast agent in tumors at relatively high spatial resolution and sufficient temporal resolution to identify a washin and a washout process. The detailed enhancement time course in each pixel is complex, depending on various physiological parameters such as blood volume, blood flow, micro-vascular permeability x surface area, volume fraction accessible to the contrast agent, interstitial fluid pressure, contrast agent diffusion and water exchange rates (8 and references cited therein).

Most malignant tumors in the breast enhance substantially within the first few minutes after a bolus injection of a contrast agent as a result of fast washin of the agent into the extracellular volume. The washin phase is then followed by a washout phase or a steady phase or a continued washin phase, depending on the vascular and tissue properties (9). Benign breast lesions may often show enhancement as well, but usually with a different pattern as compared to cancer lesions (10). The normal fibroglandular breast tissue may enhance, depending also on the hormonal status of the patient (11) but usually with a different pattern of enhancement and of lower enhancement intensity than most breast lesions.

In most DCE-MRI studies of the breast the analysis of the data has been based on empiric descriptors of the enhancement-time curves such as time to peak, peak enhancement and presence of washout. In addition, breast DCE datasets were evaluated by fitting the time curves to pharmacokinetic models that yielded physiological parameters of the model (9, 12, 13).

It is now well recognized that most cancers are highly heterogeneous and therefore high spatial resolution is required for sorting out "hot spots" with a large fraction of leaky capillaries (14). Hence, pixel by pixel analysis of high spatial resolution data is preferable. However, pixel by pixel fitting to a multi-parameter, complex equation is time consuming and it may not converge or converge to unphysiological local minimum. Furthermore, the accuracy of the fitting requires sufficient temporal resolution (15), and additional intricate and time consuming measurements of the blood arterial input function and the precontrast T1 relaxation rate.

In recent years several model free processing methods have been applied in order to overcome part of the limitations of the model based fitting methods. These methods used either an unsupervised approach that attempts to cluster unlabeled input data or a supervised approach with a learning step in which the classification system adjusts itself according to a labeled training set (16). Among these methods, factor analysis (17), principal component analysis (PCA) and independent component analysis (ICA) were applied for analyzing breast DCE datasets. Both PCA and ICA were applied for various purposes: 1. Reducing the dimensionality of the data in order to reduce the effects of artifacts and increase the signal to noise ratio (18-22); 2. Registration of DCE datasets (23); 3. Post processing fat suppression (24, 25) and 4. Identifying breast tumors and characterizing kinetic behavior in order to improve breast cancer detection and diagnosis (26-31).

Despite the marked advancements in MRI hardware and software, including multi-channel dedicated breast coils, fast acquisition sequences and computer aided software for image processing; breast DCE-MRI still suffers from high variability of radiological evaluation, particularly differentiating malignant from benign lesions (32 and references cited therein). One of the main causes of this variability is lack of standardization of the MRI protocol and the image processing method and consequently the evaluation of breast lesions. In order to reach standardization of the radiological evaluation, the protocol and processing means must be linked together and adjusted to yield quantifiable and reproducible parameters, characterizing the actual perfusion physiology.

We have previously developed a model based method that adjusts breast DCE-MRI protocols to yield standardized evaluation of lesions, termed the three time point (3TP) method (33-35). Initially, when this method was developed, it was possible to achieve high spatial resolution breast images only with long scanning times (4 min). Consequently, two critical postcontrast time points were selected and the washin and washout rates were related to the model based physiological parameters using a calculated calibration map (9). Later, when it became possible to maintain high spatial resolution and enhance the temporal resolution, we developed a processing tool for breast and prostate DCE-MRI using PCA adjusted with the 3TP parameters (29, 30, 36). In this report we describe the actual testing of the performance of a standardization process based on a 3TP+PCA hybrid method, using different scanners at two field strengths

(1.5T and 3T) and three different sequence protocols. The results demonstrate the ability of this hybrid method to achieve standardization of the radiological evaluation of breast lesions and serve as a fast and reproducible means for breast DCE image processing.

Materials and Methods

Patients

The study was approved by the Internal Review Board of Meir Medical Center, Kfar-Saba, Israel. All lesions were analyzed retrospectively. The study included three groups of patients, each scanned with a different MRI protocol as described below:

Group 1: Patients were scanned at 1.5T using 2 precontrast and 4 postcontrast time points. In 24 patients at median age 50 (range 24-80) 31 malignant lesions were detected (20 invasive ductal carcinoma (IDC), 6 invasive lobular carcinoma (ILC) and 5 ductal carcinoma *in situ* (DCIS)). In 12 patients at median age 50 (range 24-78) 12 benign lesions were detected (3 fibroadenoma and 9 fibrocystic changes).

Group 2: Patients were scanned at 1.5T using 2 precontrast and 6 postcontrast time points. In 27 patients at median age 50 (range 24-80) 40 malignant lesions were detected (25 IDC, 11 ILC and 4 DCIS) and in 3 patients (aging 26, 50 and 80) 3 benign lesions were detected.

Group 3: Patients were scanned at 3T using 2 precontrast and 7 postcontrast time points. In 20 patients at median age 52 (range 31-72) 25 malignant lesions were detected (17 IDC, 4 ILC and 4 DCIS). In 9 patients at median age 45 (range 26-65) 11 benign lesions were detected (8 fibroadenoma and 3 other benign changes).

All malignant lesions were confirmed by histopathology of biopsy or surgical specimens. Benign lesions were either confirmed by histopathology of biopsy specimens or by follow-up of more than 2 years.

MRI Protocol

The first two groups were scanned on a 1.5T scanner (Intera, Philips) and the third group was scanned on a 3T scanner (Trio, Siemens), using dedicated breast coils (with 4 or 7 Channels), applying bilateral, three-dimensional, axial and low-angle gradient-echo sequence. The contrast agent (magnetol, Soreq, Israel) was injected as a bolus at a dose of 0.1 mmol/kg. The acquisition parameters for the DCE protocol in all three scanners were determined by using the

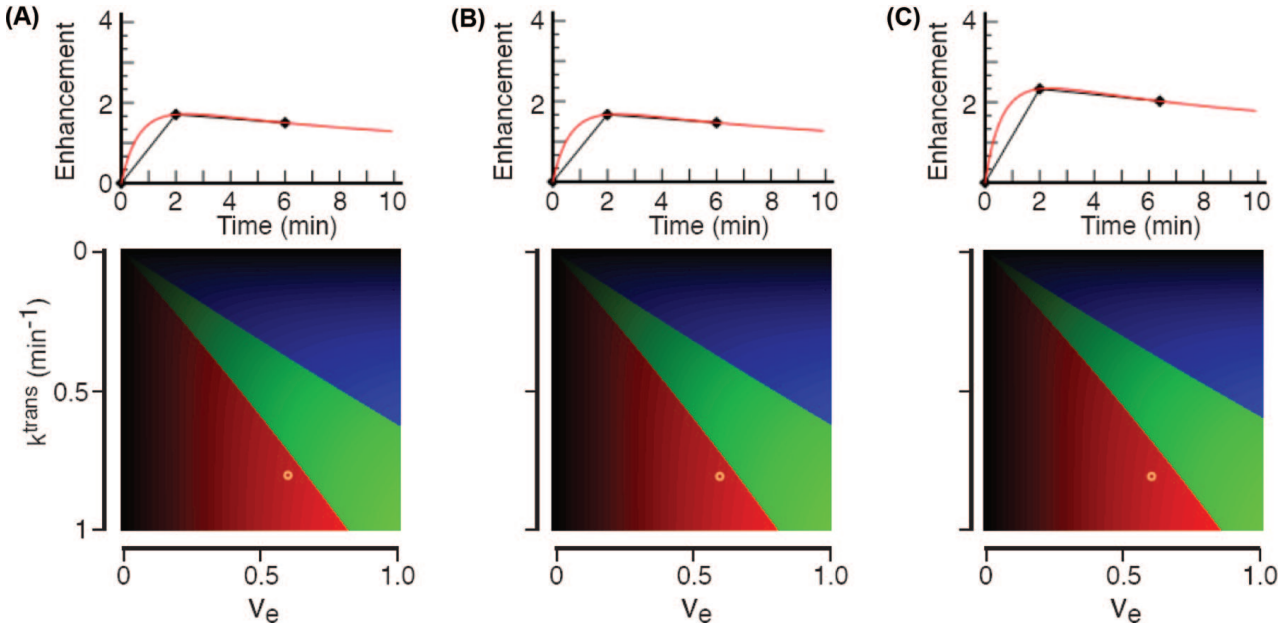

Figure 1: 3TP enhancement calibration maps for three optimized scanning parameters. **A**, **B** and **C** – Calibration map and typical enhancement curve for the scanning conditions of Group 1, 2 and 3, respectively, obtained as described in Materials and Methods. The upper enhancement curve was calculated for $k^{trans} = 0.8\,min^{-1}$ and $v_e = 0.6$, indicated by a circle on each calibration map. The calibration maps were obtained using a kinetic model and a color coded scheme (35). Color intensity indicates washin enhancement rate between precontrast time point and 1st preselected postcontrast time point. Color hue indicates enhancement washout pattern between preselected 1st and 2nd postcontrast time points: Red, decreased enhancement; Green, steady enhancement within 10% difference and Blue, increased enhancement.

3TP software for calculating the enhancement calibration map based on a dynamic model (37). In this map, the transcapillary transfer constant (k^{trans}), ranged from 0 to 1 min^{-1} and the extracellular volume fraction (v_e) accessible to the contrast agent, ranged from 0 to 1 (see Figure 1) (9, 33, 35). Note that the model assumed equal influx and outflux transcapillary transfer with efflux transcapillary transfer, $k_{ep} = k^{trans}/v_e$ (37).

The acquisition parameters of Group 1 were echo time/repetition time (TE/TR) = 4.6 msec/10 msec, flip angle 25°, field of view 34-40 cm^2, matrix 512 × 512, in-plane spatial resolution of 0.66-0.79 mm, 75 slices with slice thickness 4.8 mm and temporal resolution of 120 sec. The postcontrast time points were 2, 4, 6 and 8 min.

The acquisition parameters of Group 2 were TE/TR = 4.6 msec/11 msec, flip angle 25°, field of view 34-36 cm^2, matrix 448 × 448, in-plane spatial resolution of 0.79 mm, 70 slices with slice thickness 2.5 mm and temporal resolution of 80 sec. The postcontrast time points were 0.66, 2, 3.33, 4.66, 6 and 7.33 min.

The acquisition parameters of Group 3 were TE/TR = 2.49 msec/6.8 msec, flip angle 18°, field of view 36 cm, matrix 448 × 448, in-plane spatial resolution of 0.8 mm, 60 slices with slice thickness of 2-2.5 mm and temporal resolution of 70 sec. The postcontrast time points were 0.9, 2, 3.1, 4.2, 5.3, 6.4 and 7.5 min.

Image Processing

PCA of Cancer Test Cases: DCE intensity-scaled datasets were loaded into MATLAB® (The MathWorks, Inc., MA, USA). The intensity weighted datasets were transformed to enhancement datasets by subtraction and normalization of each pixel intensity, in the set of images according to $[I_i(t)–I_i(0)]/I_i(0)]$, where $I_i(0)$ is the precontrast intensity and $I_i(t)$ is the intensity at time t postcontrast. Localization of the lesions in the enhancement datasets was performed by an experienced breast radiologist (M.S.F.). The temporal dataset of a central slice of each lesion was selected for analysis. Delineation of the lesion region of interest (ROI) was performed on the ~2 min postcontrast enhancement images, selecting pixels above an enhancement threshold of 30%.

PCA was applied on the lesion ROI of 5-7 IDC test cases. For n time points of a DCE protocol (including 2 precontrast), n–1 enhancement time points were analyzed by PCA. The temporal signal enhancement variations v^1 to v^{n-1} for each pixel within the ROI were associated with a state vector: $u_i = (v_i^1, v_i^2, v_i^3 ... v_i^{n-1})^T$ (T-transpose). The set of all state vectors in the ROI was defined as $\Gamma = \{u_i\}, 1 \le i \le N$ with N the number of pixels in the ROI. The first-order covariance matrix, COV, was calculated according to:

$$\mathrm{COV} = \frac{1}{N}\sum_{u\in\Gamma}(u-\bar{u})(u-\bar{u})^T \quad [1]$$

$$\bar{u} = \frac{1}{N}\sum_{u\in\Gamma}u$$

A linear PCA transformation by solving $\lambda E = \mathrm{COV}\ E$ was then applied, yielding the eigenvectors $E = \{e_1, e_2 ... e_{n-1}\}$ and eigenvalues $\lambda = \{\lambda_1, \lambda_2 ... \lambda_{n-1}\}$. The n–1 eigenvectors were indexed and sorted according to their eigenvalues. For each pixel i the state vector u_i^T was then projected on the eigenvectors E so that $u_i^T = pc_i E^T$ where pc_i defines the scalar projection coefficients of the eigenvectors $(pc_i^1, pc_i^2, pc_i^3 ... pc_i^{n-1})$. The projection coefficients of each eigenvector within a defined ROI were calculated from the scalar values pc_i^j, yielding projection coefficient maps.

Construction of a Generalized Eigenvectors' Base: Examination of the eigenvectors of the IDC test cases showed high reproducibility of the first two eigenvectors and a dominant contribution of the first two eigenvectors to the signal variation. The first two eigenvectors that best represented the test cases within a group were selected for a generalized base of eigenvectors. The selection was performed by a program that calculated for each eigenvector within a group the sum of deviations of all time points from the remaining eigenvectors in the group. The eigenvector with the lowest deviation was selected for the base. Further standardization of the eigenvectors' base was obtained by constructing a scatter plot of the projection coefficients of the 1st and 2nd eigenvectors in the ROI of the test lesions and the 3TP washin (color intensity) and washout (color hue). The two orthogonal projection coefficient axes in this plot were then rotated reaching a new distribution in the scatter plot. The rotation angle was calculated by an iterative program over a large set of possible rotation angles reaching a distribution in which the positive projection coefficients of the second eigenvector coincided with the red and green 3TP coded pixels (typical to malignant regions), and the negative projection coefficients coincided with the blue 3TP coded pixels (typical to benign breast tissue).

The enhancement datasets included in each group were projected on the corresponding rotated base yielding projection coefficient maps of the first two eigenvectors. This step did not require selection of ROI, enabling fast segmentation and analysis of the kinetic features in each lesion. The projection coefficients of the first rotated eigenvector closely corresponded to the color intensity in the parametric 3TP maps

and related to k^{trans} whereas the projection coefficients of the second rotated eigenvector corresponded to the color hue in the 3TP maps related to k_{ep}.

Statistical Analysis

Within each lesion ROI we calculated the 25th, 50th (median) and 75th percentiles of the projection coefficients of the 1st and 2nd eigenvectors. In addition, for the projection coefficients of the 2nd eigenvector we calculated the percent of voxels per lesion with projection coefficients values above a threshold of zero. Receiver operating characteristic (ROC) curve analysis (MedCalc. Version 12.4.0.0.) was applied for assessing the diagnostic ability of the projection coefficients of the 2nd eigenvector. The pathology diagnostic results were used for classification and the median values of the projection coefficients, or the number of pixels above a threshold of zero, were used as predictors. The ROC curve analysis was performed for lesions in Groups 1 and 3 and for lesions in all three groups together. We did not perform ROC analysis on Group 2 lesions because of the small number of benign lesions ($n = 3$).

Results

The initial design of the DCE-MRI protocols was performed by optimizing the scanning parameters using a model based calibration map according to the 3TP method. This map relates the two physiological parameters: the (k^{trans}) and v_e to the color coding scheme of the 3TP method (Figure 1). It can be seen that the color hue and intensity distribution in the k^{trans}–v_e map is very similar in the three different calibration maps ensuring the same color coding for pixels with the same k^{trans} and v_e (see example in Figure 1 for $k^{trans} = 0.8 min^{-1}$; $v_e = 0.6$), despite the difference in the field strength, sequence parameters and time resolution.

Evaluation of the enhancement patterns using all the time points in the dynamic data (6 in Group 1, 8 in Group 2 and 9 in Group 3) was then performed by PCA of enhancement datasets in each group.

Figure 2A demonstrates a typical time evolution of an intensity scaled Group 2 dataset in a slice of the breast with IDC. The time evolution in the ROI of the IDC was used to calculate the eigenvalues (Figure 2B) and corresponding eigenvectors (Figure 2C). The highest contribution to the changes evolved from the first two eigenvalues (Figure 2B). Calculation of the projection coefficients maps of each eigenvector depicted the dominant changes due to the enhancement in the 1st and 2nd projection coefficient maps, whereas the remaining eigenvectors depicted mainly noise changes (Figure 2D).

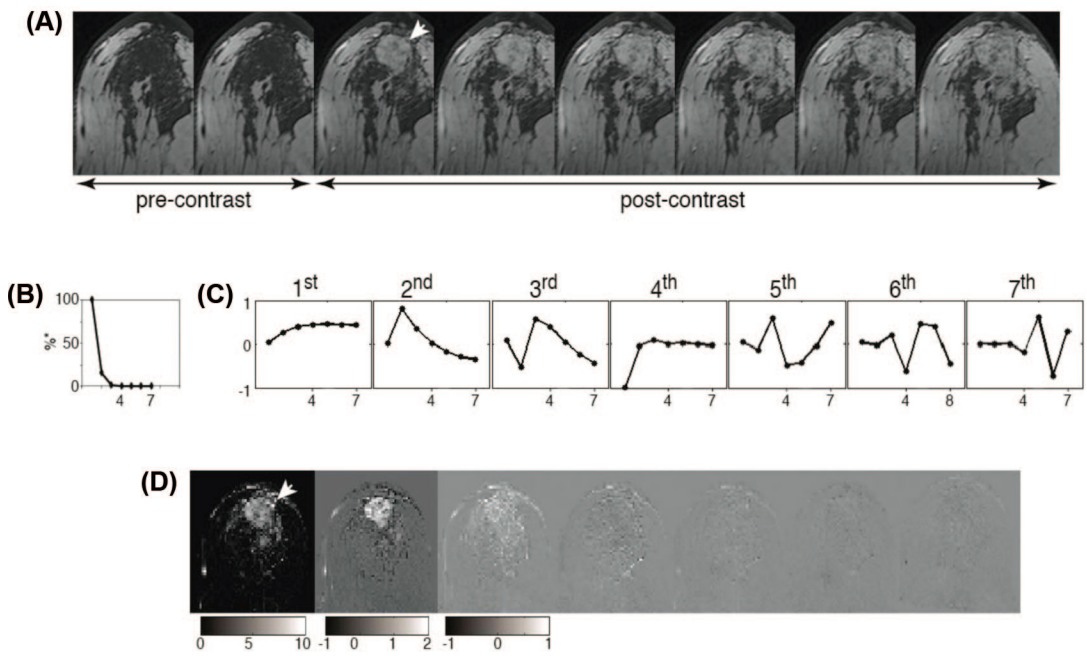

Figure 2: Principal component analysis of enhancement DCE dataset of a left breast with infiltrating ductal carcinoma. (**A**) T1 weighted images of a central slice of IDC. Time course of two precontrast and six postcontrast images recorded at 1.5T according to Group 2 scanning parameters. Arrow indicates the location of the lesion. (**B**) A plot of the PCA eigenvalues in units of percent from the value of the 1st eigenvector. Horizontal axis denotes the enhancement scan number. (**C**) A plot of the 7 eigenvectors from highest to lowest eigenvalue. Horizontal axes denote the enhancement scan number. (**D**) Projection coefficient maps of all eigenvectors from highest to lowest eigenvalue. Arrow indicates the location of the lesion.

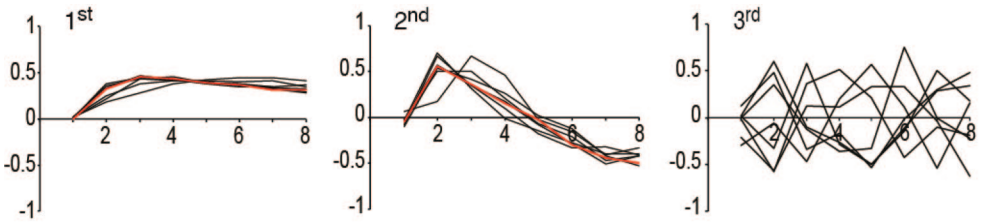

Figure 3: The first three eigenvectors obtained by PCA of 7 enhancement DCE datasets of IDC test cases recorded at 3T. The images were recorded according to Group 3 scanning parameters. The eigenvectors selected for the eigenvectors' base are marked in red. Horizontal axes denote the enhancement scan number.

Examining the PCA of the test cases indicated high reproducibility of the first two eigenvectors (with the highest eigenvalues) in each group (Figure 3) and among the groups (Figure 4). The remaining eigenvectors depicted mainly noise variations (see for example 3rd eigenvectors in Figure 3). These findings revealed that the two dominant eigenvectors, relevant for the evaluation of the DCE images, are very similar across patients.

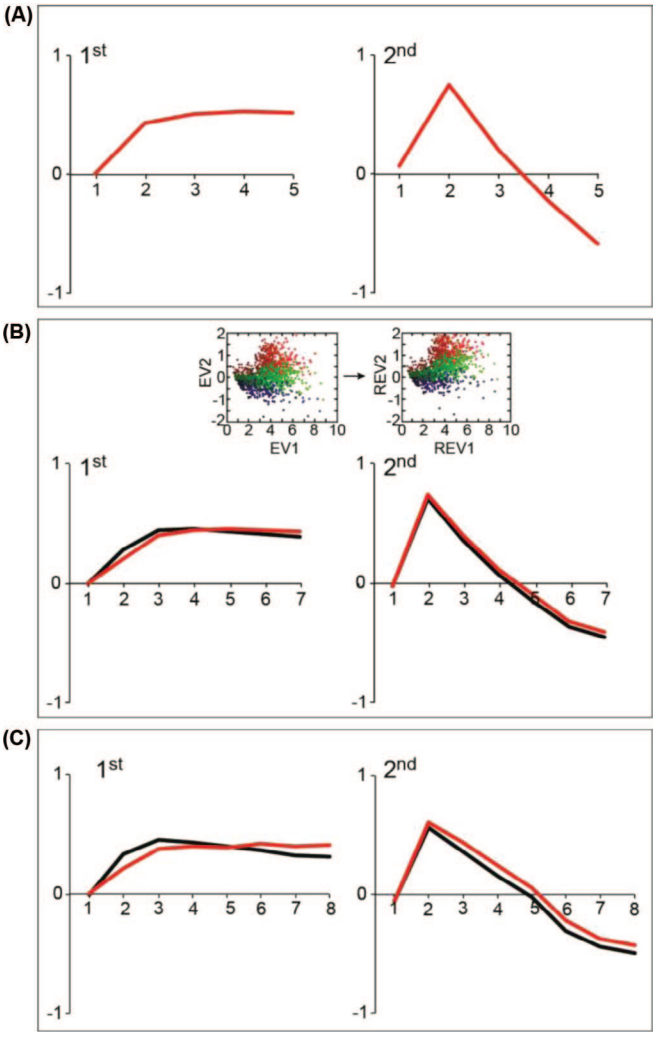

Figure 4: Eigenvectors' base of group 1(**A**), 2(**B**) and 3(**C**) calculated from 5 to 7 IDC test cases. Black, eigenvectors' base; Red, rotated eigenvectors' base. Horizontal axes denote the enhancement scan number. The inset in B demonstrates a pixel-by-pixel scatter plot of the projection coefficients of the 1st and 2nd eigenvectors and the 3TP washin rate (color intensity) and washout pattern (color hue) in ROIs of IDC test cases.

Further standardization of the PCA method was achieved by correlation with the 3TP results. We performed a pixel-by-pixel scatter plot of the projection coefficients of the 1st and 2nd eigenvectors and the 3TP washin rate (color intensity) and washout pattern (color hue) of IDC test cases (see inset in Figure 4B). The distribution in the scatter plot led us to rotate the two orthogonal eigenvectors to yield a new distribution with positive projection coefficients of the second eigenvector corresponding to red and green pixels in the 3TP map and negative values corresponding to blue pixels in the 3TP map. It was found that the eigenvectors' base of Group 1 is in full congruence with the distribution of the 3TP parameters and therefore it was not necessary to apply a rotation of the base (Figure 4A). The eigenvectors' base of Group 2 was rotated by 5.9° anti-clockwise (Figure 4B) and that of Group 3 by 11.2° anti-clockwise (Figure 4C).

The new rotated eigenvectors' base of each group served for analyzing all remaining lesions (malignant and benign) in a supervised mode. The enhancement dataset of the remaining benign and malignant cases were projected on the rotated base of each group with no need for ROI delineation and calculation of the eigenvectors. Figure 5 demonstrates typical projection coefficient maps of malignant lesions of various types and of a benign lesion – fibroadenoma. The projection coefficients of the 1st rotated eigenvector of cancer and benign lesions were always positive with the medians of the 25, 50 and 75 percentiles of all benign lesions 1.35, 2.15 and 2.95, respectively, and of all cancer lesions 1.57, 2.74 and 4.07, respectively. The tissue surrounding the lesions and normal breast tissue exhibited close to null coefficients of this eigenvector. Thus, the projection coefficient map of the 1st rotated eigenvector enabled delineation of all enhancing lesions, both malignant and benign. However, due to the high overlap of the 1st rotated projection coefficients among the benign and malignant lesions it was not possible to use it for differentiating benign from malignant lesions. In contrast, the projection coefficients of the 2nd rotated eigenvector showed a substantial

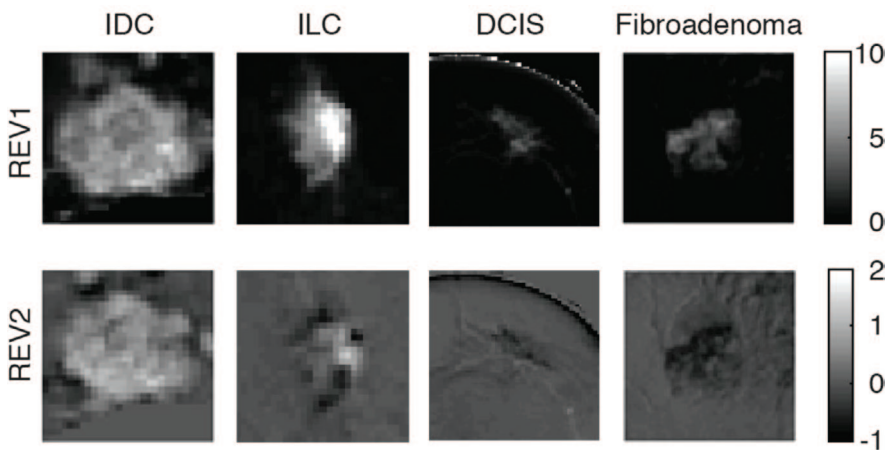

Figure 5: Typical examples of projection coefficient maps of the 1st rotated eigenvector (REV1) and the 2nd rotated eigenvector (REV2). Malignant lesions: IDC, invasive ductal carcinoma; ILC, invasive lobular carcinoma; DCIS, ductal carcinoma *in situ*. Benign lesion: fibroadenoma. Note the presence of positive values of the projection coefficients of REV1 for all lesions and a change from positive to negative values of the projection coefficients of REV2 from IDC to fibroadenoma.

Table I

Area under curve (AUC) of ROC curve analysis of lesions in Group 1 (1.5T) and Group 3 (3T) and of the lesions in all three groups.

	Median value		# of pixel above a threshold of zero	
Groups	AUC ± SD	95% confidential interval	AUC ± SD	95% confidential interval
1	0.866 ± 0.059	0.727-0.950	0.801 ± 0.069	0.651-0.907
3	0.843 ± 0.075	0.674-0.946	0.872 ± 0.068	0.709-0.962
1 + 2 + 3	0.885 ± 0.034	0.813-0.936	0.878 ± 0.034	0.805-0.931

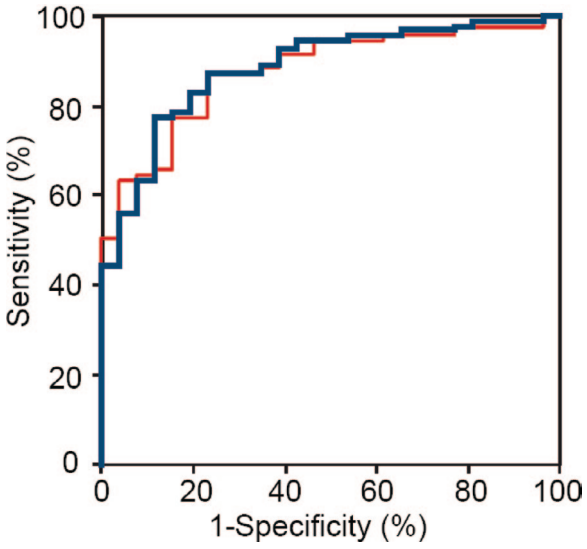

Figure 6: Receiver operating characteristic curve analysis, differentiating malignant from benign lesions. The ROC curve analysis included 93 malignant tumors and 26 benign lesion and was based on the projection coefficients of the 2nd eigenvector in the lesions. The red curve is based on using the percentage of pixels with value above a threshold >0 as predictors and the blue curve is based on using median values of the projection coefficients as predictors. Pathology diagnosis (malignant or benign) served for classification.

ability to differentiate between malignant and benign lesions as indicated by the ROC curve analysis (Table I and Figure 6). The presence of positive values of the projection coefficient of the 2nd eigenvector indicated malignancy whereas benign lesions typically exhibited negative values for this coefficient. ROC curves based on using either the median values of the 2nd rotated eigenvector or the percentage of pixels showing positive values of this coefficient, yielded a similar AUC for the 1.5T and 3T cases (Table I) enabling evaluation of all groups together (Figure 6).

Discussion

The application of PCA to process DCE datasets provides a standardized approach for data reduction; however, the radiological evaluation of the PCA output depends on the MRI protocol. It is therefore critical to develop means to standardize the analysis with respect to an optimized MRI protocol. In this report we demonstrate fusion of the 3TP method with PCA in order to achieve standardization of DCE-MRI in terms of the output parameters that quantify the contrast agent perfusion kinetics and thus, enabling objective evaluation of breast lesions. The entire scanning and image

processing procedure consisted of three main steps (Figure 7): 1. Optimizing the MRI scanning parameters according to the 3TP method; 2. Applying PCA and constructing an eigenvectors' base reflecting the perfusion kinetics and 3. Projecting DCE-MRI datasets on the eigenvectors' base and utilizing the output parameters for the radiological evaluation of lesions.

Two groups of datasets were recorded on the same 1.5T scanner and the third group was recorded on a 3T scanner, applying different acquisition parameters, including three different temporal resolutions. PCA of the dynamic datasets of test cases of invasive cancers in each group exhibited two dominant 1st and 2nd eigenvectors. Most importantly, these two eigenvectors were found to be similar across patients, confirming the standardization achieved by the 3TP+PCA method. It also led to the construction of an eigenvectors' base and analysis of new cases in a supervised mode.

Further improvement in the standardization of the eigenvectors' base in relation to the kinetic behavior was achieved by correlation of the projection coefficients of the 1st and 2nd eigenvectors with the 3TP parametric maps of invasive cancer lesions. This adjustment yielded a new rotated eigenvectors' base on which new datasets of breast DCE in each group were projected. The analysis of all the cases confirmed our previously reported results (29, 30), showing that for all groups the 1st rotated eigenvector exhibits positive projection coefficients in malignant and benign breast lesions, whereas the 2nd eigenvector exhibits positive projection coefficients in invasive cancers (IDC and ILC). This coefficient becomes lower in DCIS and is negative in most benign lesions. Overall, the results clearly showed high congruence in the ability of the three different MRI protocols to detect lesions and to differentiate benign from malignant lesions.

It should be noted that the radiological evaluation of each group was obtained using the corresponding rotated eigenvectors' base rather than calculating new eigenvectors for each case. In addition, once the eigenvectors' base was constructed, the computation of the projection coefficients provided maps over the entire breast, enabling fast segmentation and diagnosis of a large volume of datasets.

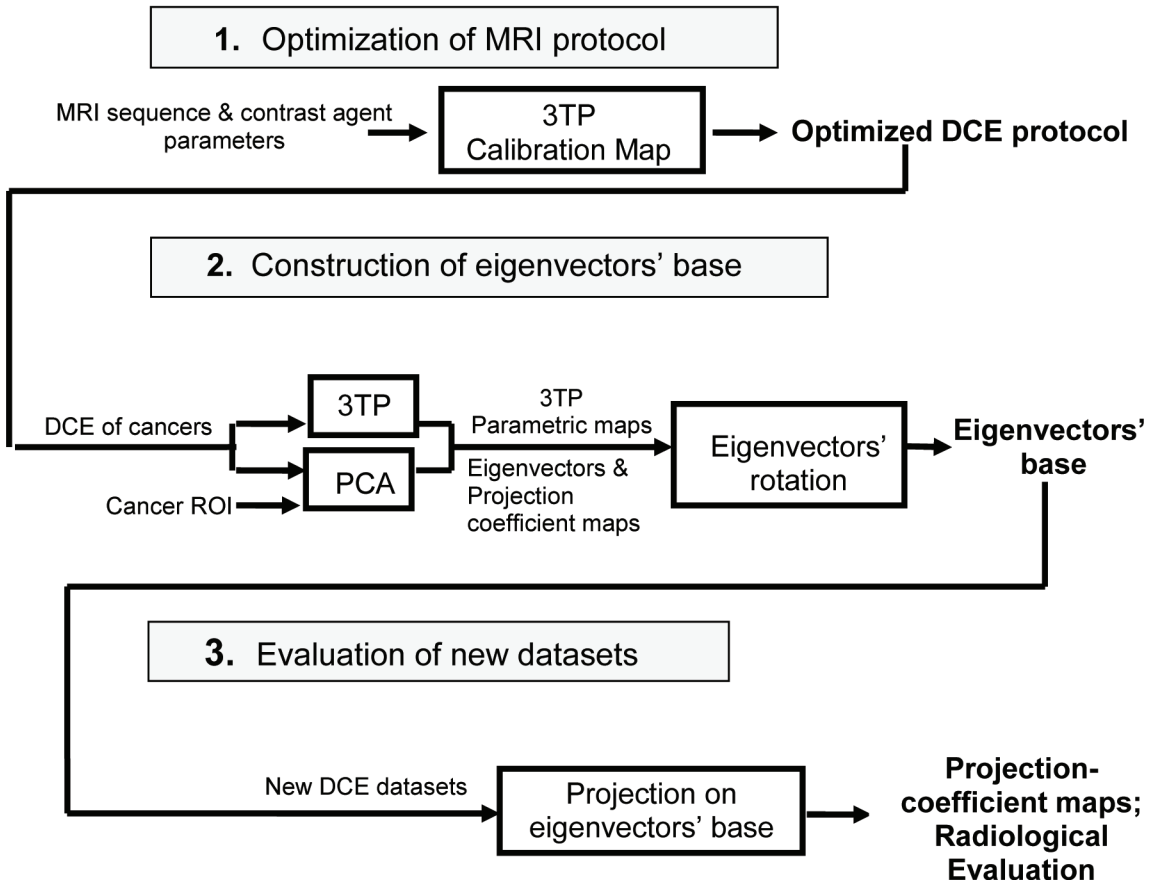

Figure 7: Flow chart of the steps required for scanning, processing and standardizing the evaluation of breast DCE datasets using the 3TP+PCA hybrid method.

The main advantages in using the 3TP+PCA hybrid method over a model-based dynamic analysis is the use of non-complex algorithms and fast and easy to implement computation procedure. PCA also assures a distinct, globally optimal solution rather than a solution that depends on the choice of model and the precision of input parameters (*i.e.*, arterial input function), as well as on the fitting accuracy. Unlike the current radiological evaluation that utilizes qualitative assessment of enhancement features and is based on the reader experience, the 3TP+PCA hybrid method provides quantitative assessment and is a reader independent method.

Previous reports on the use of breast DCE image processing, based on PCA or ICA, tested relatively small number of lesions, and hence, their diagnostic ability was not evaluated (26-28, 31). The major difference between the 3TP+PCA hybrid method and the 3TP method alone is the utilization of the entire dataset by the former method. The 3TP method selects for the washin rate a single postcontrast time point, disregarding earlier time points, and defines only three discrete regions for the washout patterns. Thus, it may overlook both washin and washout distinct enhancement features when the temporal resolution is high. In contrast, the fusion of 3TP and PCA uses the entire set of time points and the projection coefficient values of the 1st eigenvector (reflecting washin rates) can vary continuously from null to any positive value and the projection coefficients of the 2nd eigenvector (reflecting washout rates) can vary continuously from negative to positive values.

It is important to emphasize that the hybrid method did not reveal unique features in the enhancement curves for the applied temporal resolution range of 70-120 sec.

Although in the protocols of Groups 2 and 3 the first postcontrast time point was less than a minute, this did not affect the eigenvectors' curves. Thus, a temporal resolution of 1-2 min of DCE images, which enables scanning at high spatial resolution, is sufficient for the evaluation and the diagnosis of breast lesions. We can hypothesize that increasing markedly the sampling rate at the washin phase, without decreasing the spatial resolution, may change the eigenvectors and eigenvalues and slightly improve the diagnostic accuracy, as suggested from a recent study (38). However, in practical terms, most clinical MRI scanners cannot achieve today both high spatial resolution ($<1\,mm^3$) and high temporal resolution (few seconds).

Despite the standardization achieved by the 3TP+PCA method there are still intrinsic variability due to differences in the physiology of tumor perfusion, blood pharmacokinetics and experimental variations in the contrast agent injection. Distortions due to movement throughout the time course of enhancement can also affect the radiological evaluation, however, they can be reduced by using registration methods (39, 40).

In summary, using the 3TP+PCA hybrid method we have demonstrated standardization of the radiological evaluation of breast DCE examinations, for different field strength, scanning acquisition parameters and temporal resolution. The output of this method yielded projection coefficient maps that quantitatively assessed the kinetics of perfusion, enabling detection and diagnosis of breast lesions. This method can be applied as a computer aided diagnostic tool of breast cancer and be extended to diagnose malignancy in other organs, as well as monitor response to therapy.

Acknowledgement

We would like to thank Mr. Nahum Stern and Ms. Fanny Attar for their excellent technical assistance. H.D. holds the Fred and Andrea Fallek Chair for Breast Cancer Research.

References

1. Caravan P, Ellison JJ, McMurry TJ & Lauffer RB. Gadolinium (III) chelates as MRI contrast agents: structure, dynamics and applications. *Chem Rev 99*, 2293-2352 (1999).
2. Yankeelov TE & Gore JC. Dynamic contrast enhanced magnetic resonance imaging in oncology: theory, data acquisition, analysis and examples. *Curr Med Imaging Rev 3*, 91-107 (2009).
3. Moon M, Cornfeld D & Weinreb J. Dynamic contrast enhanced breast MR imaging. *Magn Reson Imagung Clin N Am 17*, 351-362 (2009). DOI: 10.1016/j.mric.2009.01.010
4. Verma S, Turkbey B, Muradyan N, Rajesh A, Cornud F, Haider MA, Choyke PL & Harisinghani M. Overview of dynamic contrast enhanced MRI in prostate cancer diagnosis and management. *Am J Roentgenol 198*, 1277-1288 (2012). DOI: 10.2214/AJR.12.8510
5. Sardanelli F, Lozzelli A & Fausto A. MR imaging of the breast: indications, established technique and new directions. *Eur Radiol 13*, N28-N36 (2003).
6. Carmeliet P & Jain RK. Angiogenesis in cancer and other diseases. *Nature 407*, 249-257 (2000).
7. Lunt SJ, Fyles A, Hill RP & Milosevic M. Interstitial fluid pressure in tumors: therapeutic barrier and biomarker of angiogenesis. *Future Oncol 4*, 793-802 (2008). DOI: 10.2217/14796694.4.6.793
8. Dadiani M, Furman-Haran E & Degani H. The Application of NMR in tumor angiogenesis research. *Progress in NMR Spectroscopy 49*, 27-44 (2006).
9. Furman-Haran E & Degani H. Parametric analysis of breast MRI. *J Comput Assist Tomogr 26*, 376-386 (2002).
10. Kaiser WA & Zeitler E. MR imaging of the breast: fast imaging sequences with and without Gd-DTPA. Preliminary observations. *Radiology 170*, 681-686 (1989).
11. Müller-Schimpfle M, Ohmenhaüser K, Stoll P, Dietz K & Claussen CD. Menstrual cycle and age: influence on parenchymal contrast medium enhancement in MR imaging of the breast. *Radiology 203*, 145-149 (1997).
12. Brix G, Kiessling F, Lucht R, Darai S, Wasser K, Delorme S & Griebel J. Microcirculation and microvasculature in breast tumors: pharmacokinetic analysis of dynamic MR image series. *Magn Reson Med 52*, 420-429 (2004).

13. Turnbull LW. Dynamic contrast enhanced MRI in the diagnosis and management of breast cancer. *NMR Biomed 22*, 28-32 (2009). DOI: 10.1002/nbm.1273
14. Furman-Haran E, Grobgeld D, Kelcz F & Degani H. Critical role of spatial resolution in dynamic contrast enhanced breast MRI. *J Magn Reson Imaging 13*, 862-867 (2001).
15. Fluckiger JU, Schabel MC & Dibella EV. The effect of temporal sampling on quantitative pharmacokinetic and three time point analysis of breast DCE-MRI. *Magn Reson Imaging 30*, 934-943 (2012). DOI: 10.1016/j.mri.2012.02.011
16. Eyal E & Degani H. Model-based and model-free parametric analysis of breast dynamic contrast enhanced MRI. *NMR Biomed 22*, 40-53 (2009).
17. Frouge C, Guinebretiere JM, Contesso G, Paola RD & Blery M. Correlation between contrast enhancement in dynamic magnetic resonance imaging of the breast and tumor angiogenesis. *Invest Radiol 29*, 1043-1049 (1994).
18. Martel AL, Ramsay E & Plewes D. Using principal components analysis to reduce the effect of streaking artifacts in dynamic PR-TRICKS images of the breast in *Proceedings of The 13th Annual Meeting of the ISMRM,* Miami, USA, p. 1861 (2005).
19. Guo J, Rosen MA & Song HK. Evaluation of principal component analysis for highly undersampled radial DCE-MRI in *Proceedings of The 15th Annual Meeting of ISMRM*, Berlin, Germany, p. 1885 (2007).
20. Martel AL, Chan RW, Ramsay E & Plewes DB. Removing under sampling artifacts in DCE-MRI studies using independent components analysis. *Magn Reson Med 59*, 874-884 (2008). DOI: 10.1002/mrm.21552
21. Lin W, Guo J, Rosen MA & Song HK. Respiratory motion compensated radial dynamic contrast enhanced (DCE)-MRI of Chest and Abdominal Lesions. *Magn Reson Med 60*, 1135-1146 (2008). DOI: 10.1002/mrm.21740
22. Balvay D, Kachenoura N, Espinoza S, Thomassin-Naggara I, Fournier LS, Clement O & Cuenod CA. Signal-to-noise ratio improvement in dynamic contrast enhanced CT and MR imaging with automated principal component analysis filtering. *Radiology 258*, 435-445 (2011). DOI: 10.1148/radiol.10100231
23. Melbourne A, Atkinson D, White MJ, Collins D, Leach M & Hawkes D. Registration of dynamic contrast enhanced MRI using a progressive principal component registration. *Phys Med Biol 52*, 5147-5156 (2007).
24. Khazen M & Leach MO. Excitation independent fat suppression for DCE MRI of breast cancer, using a multivariate statistical approach in *Proceedings of The 12th Annual Meeting ISMRM,* Kyoto, Japan, p. 830 (2004).
25. Khazen M, D'Arcy J, Collins DJ, Padhani AR & Leach MO. Assessing tumur extent and heterogeneity on T1-weighted 3D DCEMRI of breast cancer: comparative study of the computational fat suppression algorithm and quantitative pharmacokinetic (PK) modeling in *Proceeding of The 13th Annual Meeting ISMRM,* Miami, USA, p. 88 (2005).
26. Yoo SS, Gil Choi B, Han JY & Hee Kim H. Independent component analysis for the examination of dynamic contrast enhanced breast magnetic resonance imaging data: preliminary study. *Invest Radiol 37*, 647-654 (2002).
27. Twellmann T, Saalbach A, Gerstung O, Leach MO & Nattkemper TW. Image fusion for dynamic contrast enhanced magnetic resonance imaging. *Biomed Eng Online 3*, 35-56 (2004).
28. Koh TS, Thng CH, Ho JT, Tan PH, Rumpel H & Khoo JB. Independent component analysis of dynamic contrast enhanced magnetic resonance images of breast carcinoma: a feasibility study. *J Magn Reson Imaging 28*, 271-277 (2008). DOI: 10.1002/jmri.21391
29. Eyal E, Furman-Haran E, Badikhi D, Kelcz F & Degani H. Combination of model-free and model-based analysis of dynamic contrast enhanced MRI for breast cancer diagnosis. *SPIE Proc Med Img* (2008).
30. Eyal E, Badikhi D, Furman-Haran E, Kelcz F, Kirshenbaum KJ & Degani H. Principal component analysis of breast DCE-MRI adjusted with a model-based method. *J Magn Reson Imaging 30*, 989-998 (2009). DOI: 10.1002/jmri.21950
31. Saalbacha A, Langea O, Nattkemperb T & Meyer-Baesea A. On the application of (topographic) independent and treedependent component analysis for the examination of DCE-MRI data. *Biomed Signal Process Control 4*, 247-253 (2009).
32. Dorrius MD, Jansen-van der Weide MC, van Ooijen PM, Pijnappel RM & Oudkerk M. Computer-aided detection in breast MRI: a systematic review and meta-analysis. *Eur Radiol 21*, 1600-1608 (2011). DOI: 10.1007/s00330-011-2091-9
33. Degani H, Gusis V, Weinstein D, Fields S & Strano S. Mapping pathophysiological features of breast tumors by MRI at high spatial resolution. *Nature Med 3*, 780-782 (1997).
34. Furman-Haran E, Grobgeld D, Margalit R & Degani H. Response of MCF7 human breast cancer to tamoxifen: evaluation by the three time point, contrast enhanced magnetic resonance imaging method. *Clin Cancer Res 4*, 2299-2304 (1998).
35. Kelcz F, Furman-Haran E, Grobgeld D & Degani H. Clinical testing of high spatial-resolution parametric contrast enhanced MR imaging of the breast. *Am J Roentgenol 179*, 1485-1492 (2002).
36. Eyal E, Bloch BN, Rofsky NM, Furman-Haran E, Genega EM, Lenkinski RE & Degani H. Principal component analysis of dynamic contrast enhanced MRI in human prostate cancer. *Invest Radiol 45*, 174-181 (2010). DOI: 10.1097/RLI.0b013e3181d0a02f
37. Tofts PS, Brix G, Buckley DL, Evelhoch JL, Henderson E, Knopp MV, Larsson HB, Lee TY, Mayr NA, Parker GJ, Port RE, Taylor J & Weisskoff RM. Estimating kinetic parameters from dynamic contrast enhanced T1-weighted MRI of a diffusable tracer: standardized quantities and symbols. *J Magn Reson Imaging 10*, 223-232 (1999).
38. Schabel MC, Morrell GR, Oh KY, Walczak CA, Barlow RB & Neumayr LA. Pharmacokinetic mapping for lesion classification in dynamic breast MRI. *J Magn Reson Imaging 31*, 1371-1378 (2010). DOI: 10.1002/jmri.22179
39. Melbourne A, Hipwell J, Modat M, Mertzanidou T, Huisman H, Ourselin S & Hawkes DJ. The effect of motion correction on pharmacokinetic parameter estimation in dynamic contrast enhanced MRI. *Phys Med Biol 56*, 7693-7708 (2011). DOI: 10.1088/0031-9155/56/24/001
40. Hill A, Mehnert A, Crozier S, Leung C, Wilson S, McMahon K & Kennedy D. Dynamic breast MRI: image registration and its impact on enhancement curve estimation. *Conf Proc IEEE Eng Med Biol Soc 1*, 3049-3052 (2006).

Received: March 21, 2013; Revised: April 27, 2013;
Accepted: May 8, 2013